Dark Matter and Nature of Electroweak Phase Transition with an Inert Doublet

Sven Fabian,[a] **Florian Goertz,**[a] **and Yun Jiang**[a,b]

[a]Max-Planck-Institut für Kernphysik, Saupfercheckweg 1, 69117 Heidelberg, Germany
[b]TianQin Research Center for Gravitational Physics & School of Physics and Astronomy, Sun Yat-sen University (Zhuhai Campus), Zhuhai 519082, P.R. China

E-mail: fabian@mpi-hd.mpg.de, florian.goertz@mpi-hd.mpg.de, jiangyun5@sysu.edu.cn

Abstract. We provide a comprehensive and up-to-date analysis of the prospects to realize Dark Matter (DM) in the Inert Doublet Model, while simultaneously enhancing the Electroweak Phase Transition (EWPhT) such as to allow for electroweak baryogenesis. Instead of focusing on certain aspects or mass hierarchies, we perform extensive, yet fine-grained, parameter space scans, where we analyze the nature of the EWPhT in both the light and the heavy DM regions, confronting it with the amount of DM potentially residing in the lightest inert-doublet state. Thereby, we point out a viable region where a non-trivial two-step EWPhT can appear, without being in conflict with direct-detection bounds, which could leave interesting imprints in gravitational wave signatures. We propose new benchmarks with this feature as well as update benchmarks with a strong first-order transition in the light of new XENON1T limits. Moreover, taking into account these latest bounds as well as relevant collider constraints, we envisage a new region for light DM with a small mass splitting, lifting the usual assumption of exact degeneracy of the new non-DM scalars, such as to avoid collider bounds while providing a fair DM abundance over a rather large DM mass range. This follows from a detailed survey of the impact of co-annihilations on the abundance, dissecting the various channels.

Contents

1 Introduction and Setup

The presence of a baryon-asymmetric universe and of non-luminous Dark Matter (DM) leads to the conclusion that our current understanding of nature, and thus the Standard Model of Particle Physics (SM), is incomplete. In consequence, although in the past decades the SM was very successful in describing the microscopic properties and interactions of the elementary particles found so far, with the latest highlight being the discovery of the predicted Higgs boson at the LHC in 2012, it needs to be extended to agree with these findings. On the observational side, the energy budget of the universe can be characterized by the ΛCDM model as the standard picture of Big Bang Cosmology, based on general relativity, which includes the cosmological constant Λ and Cold Dark Matter (CDM), and delivers a good fit to the plethora of cosmological observations, starting from six parameters [1]. However, what is the *nature* of DM (or of the cosmological constant) is still unsettled and cannot be addressed within the SM. It is thus hoped that a microscopic theory extending the SM will eventually be unveiled, that could resolve this issues. The same is true for the dynamics behind the observed non-vanishing baryon-density, which cannot be generated via SM physics - lacking a strong first-order Electroweak Phase Transition (EWPhT), to allow for out-of-equilibrium dynamics, and a sufficient amount of CP violation.

While we will comment more on means to generate additional CP violation later, the main focus of this article will be to investigate DM Physics as well as the EWPhT dynamics comprehensively in the framework of the Inert Doublet Model (IDM), which furnishes a very clear and predictive extension of the SM. Here, the Higgs sector of the SM is augmented with an electroweak (EW) doublet, odd under a $\mathbb{Z}_2$ symmetry and with vanishing vacuum expectation value (vev) at zero temperature, which naturally includes a DM candidate as well as the potential to enhance the EWPhT. We aim for accommodating the correct DM abundance and the presence of a strong first-order EWPhT simultaneously, thereby going through the various possibilities, while meeting all relevant constraints from collider searches and cosmology. Even though the IDM has been subject to several analyses, a comprehensive scan of the whole parameter space regarding the nature of the EWPhT and a successful DM physics, including up-to-date constraints and considering the full range of (DM) masses, would be useful. Moreover, a detailed exploration of the potential to achieve a successful two-step EWPhT and of its particularities is still lacking. Both will be provided in this article, including a detailed treatment of finite temperature effects, employing thermal resummation.

This article is organized as follows. In the remainder of this section we introduce the model, summarize important constraints from EW precision data and exotic SM Higgs decay as well as analyze the IDM scalar potential at finite temperature. Subsequently, in Sec. 2, we study comprehensively the DM physics over a large range of masses, deriving the relic abundance taking carefully into account the effect of different co-annihilation channels and incorporating most recent limits from DM direct detection (DD), which turn out to close recently still available mass ranges. On the other hand, we propose a new viable spectrum with small mass splitting that can lead to a proper amount of DM without being confined to narrow stripes in the DM mass. In Sec. 3 we explore various particularities of the EWPhT in the IDM, presenting for the first time a detailed, fine-grained, survey of the parameter space regarding the nature of the EWPhT, which we find to be a two-step transition in well-constrained stripes of parameters, fulfilling all relevant bounds and providing a viable DM abundance. In turn, we define a new set of benchmarks where we trace the EWPhT, arriving at the proper EW vacuum in a non-trivial way, which are expected to lead to interesting gravitational wave (GW) signatures with multi-peaked spectra. Finally, we conclude in Sec. 4.

1.1 The Inert Doublet Model

In the IDM (see, *e.g.*, Refs. [2, 3]), an additional EW doublet H_2 is added to the SM Higgs doublet H_1, reading

$$H_1 = \frac{1}{\sqrt{2}} \begin{pmatrix} \phi^+ \\ h + i\phi \end{pmatrix} \quad , \quad H_2 = \begin{pmatrix} H^+ \\ (H + iA)/\sqrt{2} \end{pmatrix} . \tag{1.1}$$

Here, h is the SM-like neutral Higgs field,[*] with the vev $\langle h \rangle \equiv v \approx 246$ GeV at zero temperature, ϕ^+, $\phi^- = \phi^{+*}$, and ϕ are the EW Goldstone bosons, $H^\pm$ and H are new, charged and neutral, CP-even scalars, while A is a new CP-odd scalar (acknowledging that it is actually not possible to unambiguously assign definite CP properties to the neutral states of the second doublet due to the absence of suited processes [4]). Imposing a discrete $\mathbb{Z}_2$ symmetry, under which H_2 is odd while all the SM fields are even, prevents the lightest $\mathbb{Z}_2$-odd particle from decaying into SM particles. Thus, it plays the role of the DM candidate in this model.

The resulting scalar potential reads (see, *e.g.*, [4])

$$\begin{aligned}
V &= \mu_1^2 |H_1|^2 + \mu_2^2 |H_2|^2 + \lambda_1 |H_1|^4 + \lambda_2 |H_2|^4 \\
&+ \lambda_3 |H_1|^2 |H_2|^2 + \lambda_4 \left| H_1^\dagger H_2 \right|^2 + \frac{\lambda_5}{2} \left[\left(H_1^\dagger H_2 \right)^2 + \text{h.c.} \right] ,
\end{aligned} \tag{1.2}$$

with μ_2, λ_2, λ_3, λ_4, λ_5 as free, real, parameters and the remaining Lagrangian coincides with the SM one, up to gauge invariant kinetic terms for the new doublet. In particular, due to $\mathbb{Z}_2$-invariance, no new Yukawa couplings appear. Using the notations for the Higgs portal couplings

$$\lambda_{345} \overset{\text{def}}{=} \lambda_3 + \lambda_4 + \lambda_5 \quad , \quad \bar{\lambda}_{345} \overset{\text{def}}{=} \lambda_3 + \lambda_4 - \lambda_5 = \lambda_{345} - 2\lambda_5 \tag{1.3}$$

and employing Landau gauge ($\xi = 0$), the mass matrices for the neutral scalars, h and H, the pseudoscalar states, ϕ and A, and for the charged scalars, $\phi^\pm$ and $H^\pm$, are given by

$$M_S^2 = \begin{pmatrix} 2\lambda_1 v^2 & 0 \\ 0 & \mu_2^2 + \lambda_{345} v^2/2 \end{pmatrix}, \ M_P^2 = \frac{1}{2} \begin{pmatrix} 0 & 0 \\ 0 & \bar{\lambda}_{345} v^2 + 2\mu_2^2 \end{pmatrix}, \ M_\pm^2 = \frac{1}{2} \begin{pmatrix} 0 & 0 \\ 0 & \lambda_3 v^2 + 2\mu_2^2 \end{pmatrix}, \tag{1.4}$$

---

[*]With some abuse of notation, we will use the same name later for the physical fluctuation around the vev.

from which the mass eigenvalues can be read off trivially[†]. We note that the portal parameters can be expressed in terms of these masses and λ_{345} via

$$\lambda_3 = \lambda_{345} + 2\frac{m_{H^\pm}^2 - m_H^2}{v^2} \quad , \quad \lambda_4 = \frac{m_A^2 + m_H^2 - 2m_{H^\pm}^2}{v^2} \quad , \quad \lambda_5 = \frac{m_H^2 - m_A^2}{v^2} \, , \quad (1.5)$$

such that, eliminating also μ_2 via Eq. (1.4), we are left with the new set of free parameters $\{\lambda_2, \lambda_{345}, m_H, m_{H^\pm}, m_A\}$, which we will employ in the following.

We already observe that, due to the new couplings being real, the IDM alone does not induce additional CP violation, which is however required in order to allow for EW baryogenesis [5]. In consequence, we envisage additional CP violating sources, which we think of agnostically as higher-dimensional operators in an effective field theory (EFT), sticking to the field content introduced in Eq. (1.1).[‡] Some possible operators are collected in

$$\mathcal{L}_{\mathcal{CP}} \supset C_{H\tilde{F}}|H_1|^2 \tilde{F}_{\mu\nu}^I F^{I\,\mu\nu} + C_{qH}|H|^2 \bar{q}_L H q_R + C_{H_2\tilde{F}}|H_2|^2 \tilde{F}_{\mu\nu}^I F^{I\,\mu\nu} \, , \quad (1.6)$$

with $F_{\mu\nu}^I$ denoting EW gauge bosons, where the first two types of operators have been studied extensively in the literature [9–12][§]. Since they both contribute significantly to electric dipole moments (see, *e.g.*, Ref. [11]), it could be interesting to consider the third operator, which in analogy to the analysis performed in Ref. [9] could induce appreciable CP violation at finite temperature for $C_{H_2\tilde{F}} \sim (\text{TeV})^{-2}$. We will comment on its impact on the DM physics in our analysis below. Finally, we note that a comprehensive study of the IDM could also be considered as a first step to a general survey of the possibility to simultaneously realize DM and EW baryogenesis, in extended scalar sectors - either linking the DM candidate via SU(2) quantum numbers to the SM, as in the IDM, or moving the DM into a singlet-like dark sector, potentially coupled to the SM via a singlet mediator, where one could also employ a 'model-independent' framework such as the extended Dark Matter EFT [13].

1.2 Theoretical Constraints and Bounds from Electroweak Precision and Higgs Data

In our analysis of the IDM, we apply theoretical constraints, such as vacuum stability and perturbative unitarity, as well as experimental bounds both from EW precision data and from exotic SM Higgs decays. Vacuum stability requires the four relations (see, *e.g.*, Ref. [4])

$$\lambda_1 > 0 \quad , \quad \lambda_2 > 0 \quad , \quad \lambda_3 > -2\sqrt{\lambda_1\lambda_2} \quad , \quad \lambda_3 + \lambda_4 - |\lambda_5| > -2\sqrt{\lambda_1\lambda_2} \, , \quad (1.7)$$

and a charge-breaking vacuum is avoided by satisfying

$$\lambda_4 - |\lambda_5| < 0 \, . \quad (1.8)$$

The conditions for perturbative unitarity read $|c_i| < 8\pi$, with [4]

$$c_{1,2} = \lambda_3 \pm \lambda_4 \quad , \quad c_{3,4} = -3\lambda_1 - 3\lambda_2 \pm \sqrt{9\left(\lambda_1 - \lambda_2\right)^2 + \left(2\lambda_3 + \lambda_4\right)^2} \, ,$$
$$c_{5,6} = \lambda_3 \pm \lambda_5 \quad , \quad c_{7,8} = -\lambda_1 - \lambda_2 \pm \sqrt{\left(\lambda_1 - \lambda_2\right)^2 + \lambda_5^2} \, , \quad (1.9)$$
$$c_{9,10} = \lambda_3 + 2\lambda_4 \pm 3\lambda_5 \quad , \quad c_{11,12} = -\lambda_1 - \lambda_2 \pm \sqrt{\left(\lambda_1 - \lambda_2\right)^2 + \lambda_4^2} \, .$$

[†]For calculating the one-loop potential, these matrices will later by generalized with (non-diagonal) field-dependent entries.

[‡]For explicit extensions of the IDM with further scalars to allow for CP violation see, *e.g.*, [6–8].

[§]Beyond that, Ref. [11] provides a systematic survey of new sources of CP violation in the SMEFT in the context of successful EW baryogenesis.

Moreover, since the decay widths of the EW gauge bosons are measured to high accuracy and no hint for new physics was found in LEP data, potential decays of the $W^\pm$ or Z into states of the additional doublet H_2 are excluded in our analysis by constraining the mass spectra to [4]

$$m_H + m_{H^\pm} > m_{W^\pm} \;\; , \;\; m_A + m_{H^\pm} > m_{W^\pm} \;\; , \;\; m_H + m_A > m_Z \;\; , \;\; 2m_{H^\pm} > m_Z \; . \tag{1.10}$$

Finally, a reinterpretation of the LEP-II data gives rise to the exclusion of an intersection of mass ranges, which can be evaded by fulfilling one of the following conditions [4, 14–16]

$$m_H > 80 \text{ GeV} \;\; \cup \;\; m_A > 100 \text{ GeV} \;\; \cup \;\; m_A - m_H < 8 \text{ GeV} \, , \tag{1.11}$$

in addition to the general bound

$$m_{H^\pm} > 70 \text{ GeV} \, , \tag{1.12}$$

from searches for charged Higgs pair production.

For a general parametrization of corrections to EW precision observables, the three oblique parameters S, T and U have been introduced in Ref. [17] and are defined to vanish in the absence of new physics [18]. Assuming U to vanish, the other two contributions are given by [3, 4]

$$S = \frac{1}{72\pi \left(x_2^2 - x_1^2\right)^3} \left[x_2^6 f_a\left(x_2\right) - x_1^6 f_a\left(x_1\right) + 9x_1^2 x_2^2 \left(x_2^2 f_b\left(x_2\right) - x_1^2 f_b\left(x_1\right)\right) \right]$$
$$T = \frac{1}{32\pi^2 \alpha v^2} \left[f_c\left(m_{H^\pm}^2, m_A^2\right) + f_c\left(m_{H^\pm}^2, m_H^2\right) - f_c\left(m_A^2, m_H^2\right) \right] \tag{1.13}$$

with the electromagnetic coupling constant $\alpha \approx 1/127$ at the scale of the Z boson mass and

$$f_a\left(x\right) \stackrel{\text{def}}{=} -5 + 12\ln x \;\; , \;\; f_b\left(x\right) \stackrel{\text{def}}{=} 3 - 4\ln x \;\; , \;\; f_c\left(x, y\right) \stackrel{\text{def}}{=} \begin{cases} \frac{x+y}{2} - \frac{xy}{x-y}\ln\frac{x}{y} & \text{for } x \neq y \\ 0 & \text{for } x = y \end{cases} \, , \tag{1.14}$$

where

$$x_1 \stackrel{\text{def}}{=} \frac{m_H}{m_{H^\pm}} \;\; , \;\; x_2 \stackrel{\text{def}}{=} \frac{m_A}{m_{H^\pm}} \, . \tag{1.15}$$

Employing the measured SM Higgs mass $m_h = 125$ GeV, the best fit with $U = 0$ yields [18]

$$S = 0.06 \pm 0.09 \;\; , \;\; T = 0.10 \pm 0.07 \, . \tag{1.16}$$

From Eqs. (1.13) and (1.14) one can for example inspect that a large splitting between $m_{H^\pm}$ and m_A would induce sizable corrections to the T parameter, violating the above constraints.

The final constraint arises from the absence of exotic Higgs decays, leading to an upper limit on the branching ratio of [19, 20]

$$\text{BR}\left(h \to \text{inv.}\right) \stackrel{\text{def}}{=} \frac{\Gamma\left(h \to \text{inv.}\right)}{\Gamma\left(h \to \text{inv.}\right) + \Gamma\left(h \to \text{SM}\right)} < \begin{cases} 0.26 \text{ from ATLAS} \\ 0.19 \text{ from CMS} \end{cases} \tag{1.17}$$

at 95% confidence level with the decay width

$$\Gamma\left(h \to \text{inv.}\right) = \frac{\left(\lambda_{345} m_W\right)^2}{8\pi g_W^2 m_h} \sqrt{1 - 4\left(\frac{m_H}{m_h}\right)^2} \, , \tag{1.18}$$

where g_W is the weak coupling constant, and the theoretical SM Higgs width reads [21]

$$\Gamma\left(h \to \text{SM}\right) = 4.07 \text{ MeV}^{+4.0\%}_{-3.9\%} \, . \tag{1.19}$$

All these constraints will be implemented in our numerical analysis in Sections 2 and 3.

1.3 Finite Temperature Effects and Electroweak Phase Transition

To investigate the EWPhT in the subsequent two-field analysis, concepts of finite-temperature QFT will be employed - but first we will add the zero-temperature one-loop potential to the tree-level potential in Eq.(1.2), with the corresponding Coleman-Weinberg (CW) potential in Landau gauge and $\overline{\text{MS}}$-scheme reading

$$V_{\text{CW}}(h, H) = \sum_i \frac{n_i}{64\pi^2} \hat{m}_i^4(h, H) \left[\ln\left(\frac{\hat{m}_i^2}{Q^2} \right) - C_i \right] . \tag{1.20}$$

Here, $i = W^\pm, Z, t, h, H, \phi, A, \phi^\pm, H^\pm$, where we just kept the most massive top quark,[¶] Q is the renormalization scale, n_i denote the number of bosonic and fermionic degrees of freedom, and C_i are renormalization-scheme dependent constants. The latter two are given by $n_W = 6$, $n_Z = 3$, $n_t = -12$, $n_\Phi = 1$, $n_{\Phi^\pm} = 2$ and $C_W = C_Z = 5/6$, $C_t = C_\Phi = C_{\Phi^\pm} = 3/2$ with $\Phi = h, H, A, \phi$ and $\Phi^\pm = H^\pm, \phi^\pm$.

The field-dependent squared masses, entering Eq. (1.20), are given by

$$\hat{m}_V^2(h, H) = \frac{h^2 + H^2}{v^2} m_V^2 \quad , \quad \hat{m}_f^2(h) = \frac{h^2}{2} y_f^2, \tag{1.21}$$

for gauge bosons $V = W^\pm, Z$ and fermions, respectively, were m_V are the masses at zero temperature, and y_f the corresponding Yukawa couplings. The remaining terms are obtained as the eigenvalues of the scalar bosons' mass matrices

$$\begin{aligned}
\widehat{M}_S^2 &= \frac{1}{2} \begin{pmatrix} 6\lambda_1 h^2 - 2\lambda_1 v^2 + \lambda_{345} H^2 & 2hH\lambda_{345} \\ 2hH\lambda_{345} & 6\lambda_2 H^2 + \lambda_{345} h^2 + 2\mu_2^2 \end{pmatrix} \\
\widehat{M}_P^2 &= \frac{1}{2} \begin{pmatrix} 2\lambda_1 h^2 - 2\lambda_1 v^2 + \bar{\lambda}_{345} H^2 & 2hH\lambda_5 \\ 2hH\lambda_5 & 2\lambda_2 H^2 + \bar{\lambda}_{345} h^2 + 2\mu_2^2 \end{pmatrix} \\
\widehat{M}_\pm^2 &= \frac{1}{2} \begin{pmatrix} 2\lambda_1 h^2 - 2\lambda_1 v^2 + \lambda_3 H^2 & hH(\lambda_4 + \lambda_5) \\ hH(\lambda_4 + \lambda_5) & 2\lambda_2 H^2 + \lambda_3 h^2 + 2\mu_2^2 \end{pmatrix} ,
\end{aligned} \tag{1.22}$$

which coincide with (1.4) in the EW ($T = 0$) vacuum $(h, H) = (v, 0)$.

To compensate shifts of the vacuum due to one-loop corrections, the counterterm potential

$$V_{\text{CT}}(h, H) = \delta m_h^2 h^2 + \delta m_H^2 H^2 + \delta\lambda_1 h^4 \tag{1.23}$$

is assumed with coefficients following from the renormalization conditions

$$\begin{aligned}
\left. \frac{\partial V_{\text{CT}}}{\partial h} \right|_{\text{vev}} &= -\left. \frac{\partial V_{\text{CW}}}{\partial h} \right|_{\text{vev}} \\
\left. \frac{\partial^2 V_{\text{CT}}}{\partial h^2} \right|_{\text{vev}} &= \left(-\frac{\partial^2 V_{\text{CW}}|_{n_{\phi(\pm)}=0}}{\partial h^2} + \frac{1}{32\pi^2} \sum_{i=\phi,\phi^\pm} \frac{\partial^2 \hat{m}_i^2(h, H)}{\partial h^2} \ln \frac{m_{\text{IR}}^2}{Q^2} \right)\Bigg|_{\text{vev}} \\
\left. \frac{\partial^2 V_{\text{CT}}}{\partial H^2} \right|_{\text{vev}} &= \left(-\frac{\partial^2 V_{\text{CW}}|_{n_{\phi(\pm)}=0}}{\partial H^2} + \frac{1}{32\pi^2} \sum_{i=\phi,\phi^\pm} \frac{\partial^2 \hat{m}_i^2(h, H)}{\partial H^2} \ln \frac{m_{\text{IR}}^2}{Q^2} \right)\Bigg|_{\text{vev}} .
\end{aligned} \tag{1.24}$$

While this fixes the renormalization of the masses $m_{h,H}$ of the SM Higgs and the DM particle, as well as the SM coupling λ_1, the new couplings λ_2 and λ_{345} are running $\overline{\text{MS}}$ couplings and

---

[¶]We explicitly checked that the contributions from the bottom quark and the tau lepton are very small.

the masses $m_{A,H^\pm}$ are assumed to be one-loop corrected. The second derivatives of V_{CW} contain in principle ill-defined terms, due to the inclusion of Goldstone modes that contribute at finite temperature but are massless at $T = 0$ in the Landau gauge, leading to IR divergences (see, *e.g.*, Ref. [22]). These expressions are subtracted, introducing an IR cutoff $m_{\mathrm{IR}}^2 = m_h^2$. This is realized in Eq. (1.24) above effectively by removing the Goldstone modes from the CW potential in the second and third line and adding instead the regular sums over Goldstone modes on the right-hand sides.

We now move on to include finite temperature effects, captured by the one-loop CW potential derived including thermal corrections to the n-point functions [23], reading

$$
V_T\left(h, H\right) = \frac{T^4}{2\pi} \left[\sum_i n_i^{\mathrm{B}} J_{\mathrm{B}} \left(\frac{\tilde{m}_i^2\left(h, H, T\right)}{T^2} \right) + \sum_i n_i^{\mathrm{F}} J_{\mathrm{F}} \left(\frac{\tilde{m}_i^2\left(h, H, T\right)}{T^2} \right) \right] , \tag{1.25}
$$

with the sums running over all viable bosons and fermions, respectively. The corresponding thermal functions are defined as [24]

$$
J_{\mathrm{B/F}}\left(x\right) \stackrel{\mathrm{def}}{=} \pm \int_0^\infty \mathrm{d}t \; t^2 \ln\left[1 \mp e^{-\sqrt{t^2+x}}\right] = \lim_{N \to \infty} \mp \sum_{l=1}^N \frac{(\pm 1)^l x}{l^2} K_2\left(\sqrt{x}l\right) \tag{1.26}
$$

and can be well approximated by truncating the infinite sum at $N = 5$, according to Ref. [25].

Since at the relevant temperatures of the phase transition, temperature-enhanced corrections spoil the convergence of the perturbative expansion, a resummation of such contributions is required. The problematic corrections can in fact be included by resumming the leading daisy self-energy diagrams, which is accounted for in Eq. (1.25) by dressing the field-dependent masses with thermal corrections [26, 27] $\hat{m}_i^2\left(h, H\right) \to \tilde{m}_i^2\left(h, H, T\right)$. The squared scalar mass matrices in (1.22) now become $\widetilde{M}_X^2 \equiv \widehat{M}_X^2 + \widehat{\Pi}(T)$, $X = S, P, \pm$, with the 2×2 diagonal matrix $\widehat{\Pi}$, derived from the low-energy limit of the respective two-point functions, with components

$$
\begin{aligned}
\widehat{\Pi}_{11}\left(T\right) &= \frac{T^2}{24} \left(6y_t^2 + 6y_b^2 + 2y_\tau^2 + \frac{9}{2}g_W^2 + \frac{3}{2}g'^2 + 12\lambda_1 + 4\lambda_3 + 2\lambda_4 \right) \\
\widehat{\Pi}_{22}\left(T\right) &= \frac{T^2}{24} \left(\frac{9}{2}g_W^2 + \frac{3^\backprime}{2}g'^2 + 12\lambda_2 + 4\lambda_3 + 2\lambda_4 \right) .
\end{aligned} \tag{1.27}
$$

The transversal parts of the SM gauge bosons are not affected by finite-temperature corrections, whereas the squared Debye masses for the longitudinal components read [25]

$$
\tilde{m}_{W_L}^2 = \frac{h^2 + H^2}{v^2}m_W^2 + 2g_W^2T^2, \;\; \tilde{m}_{Z_L,\gamma_L}^2 = \frac{h^2 + H^2}{8}\left(g_W^2 + g'^2\right) + \left(g_W^2 + g'^2\right)T^2 \pm \Delta , \tag{1.28}
$$

with now $n_{W_L} = 2$, $n_{Z_L} = n_{\gamma_L} = 1$, $C_{W_L} = C_{Z_L} = 3/2$, $C_{\gamma_L} = 0$ and the squared substitution

$$
\Delta^2 \stackrel{\mathrm{def}}{=} \frac{\left(h^2 + H^2 + 8T^2\right)^2}{64}\left(g_W^2 + g'^2\right)^2 - g_W^2 g'^2 T^2 \left(h^2 + H^2 + 4T^2\right) . \tag{1.29}
$$

In a one-step first-order EWPhT, $\langle h \rangle$ departs from zero at the critical temperature T_c at which the minimum at the origin and the minimum at $v_c > 0$ are degenerate. The strength ξ of such EWPhT can be estimated via the critical temperature and the corresponding field value as

$$
\xi \stackrel{\mathrm{def}}{=} \frac{v_c}{T_c} . \tag{1.30}
$$

Allowing for an intermediate departure of $\langle H \rangle$ from zero leads to a two-step EWPhT. This departure takes place at a temperature that we will denote by T_1 and the departure of $\langle h \rangle$ from zero occurs in turn at a temperature $T_2 < T_1$. Thus, it is possible to define two EWPhT strengths $\xi_{1,2}$ accounting for the first and second transition, respectively, which we take as

$$\xi_j \stackrel{\text{def}}{=} \frac{\sqrt{\langle h \rangle_j^2 + \langle H \rangle_j^2}}{T_j} \tag{1.31}$$

with $j \in \{1,2\}$ and the corresponding vevs $\langle h \rangle_j , \langle H \rangle_j$ eventually emerge at the transition temperatures T_j. Note that the definition of the EWPhT strength in Eq.(1.31) also holds in the case of a one-step EWPhT. Although the correct criterion for a strong EWPhT in the context of an additional doublet as well as its gauge dependence is not comprehensively clarified yet, we assume such an EWPhT capable to allow for EW baryogenesis to be present for $\xi_j \geq 1$. While different definitions of ξ_j, compared to Eq. (1.31), could be envisaged for a two-step transition, a crucial quantity for phase transitions in the context of EW baryogenesis is the EW sphaleron rate. These sphalerons are in fact sufficiently suppressed for $\xi_j \gtrsim 1$. So with the definition above, a sufficient criterion should be that both $\xi_1 \gtrsim 1$ and $\xi_2 \gtrsim 1$, *i.e.*, an accumulated baryon abundance at the first transition would not be washed out during the second. Still, the question of defining the best-suited criterion invites for further investigation.

2 Dark Matter Physics

The IDM naturally features a promising DM candidate, represented by the lightest $\mathbb{Z}_2$-odd scalar, given that it is electromagnetically neutral. In the following we will assume that this role is played by the CP even state H. In the light of DM phenomenology (and EWPhT in the subsequent analysis), the exchange $H \leftrightarrow A$ for the DM particle along with $\lambda_{345} \leftrightarrow \bar{\lambda}_{345}$ gives rise to the same results (see, *e.g.*, Ref. [4]). As it will turn out, in relevant regions of the parameter space co-annihilations of H with other states will need to be considered in calculating the relic-abundance.[‖] This can be straightforwardly included into the Boltzmann equation, describing the evolution of the DM number density n_H, [28, 29]

$$\frac{\mathrm{d} n_H}{\mathrm{d} t} = -3 H n_H - \langle \sigma_{\text{eff}} v \rangle \left[n_H^2 - \left(n_H^{\text{eq}} \right)^2 \right] , \tag{2.1}$$

employing the effective thermally averaged annihilation cross section times velocity

$$\langle \sigma_{\text{eff}} v \rangle \stackrel{\text{def}}{=} \sum_{j=1}^{N} \langle \sigma v \rangle_{Hj} \frac{n_H^{\text{eq}} n_j^{\text{eq}}}{(n^{\text{eq}})^2} , \tag{2.2}$$

which takes co-annihilations into account. Here, j runs over all N potential co-annihilating states. Assuming a Maxwell-Boltzmann distribution, the particle density n^{eq} in thermal equilibrium is given by

$$n^{\text{eq}} = \sum_i n_i^{\text{eq}} = \frac{T}{2\pi^2} \sum_i g_i m_i^2 K_2 \left(\frac{m_i}{T} \right) , \tag{2.3}$$

with the temperature T and the mass m_i and degrees of freedom g_i of the non-SM particles. For the computation of the relic abundance Ωh^2 (and the DD cross section), we employ the

---

[‖] Such co-annihilations can appear quite naturally in models with additional weak multiplets.

package micrOMEGAs [30] to solve the Boltzmann Equation, together with the CalcHEP package [31], delivering also the bare cross sections σ as well as the thermally averaged annihilation cross sections. Below, we will use the fit $\Omega h^2 = 0.1200(12)$ for the relic abundance with the reduced Hubble expansion rate $h = 0.674(5)$ from Ref. [32], denoting the central value as Ωh^2_{best}.

The resulting viable slices of parameter space for three mass spectra, defined by the splittings $\Delta m \equiv m_{A,H^\pm} - m_H$, that neither violate any of the theoretical constraints discussed in Sec. 1.2, nor exceed the measured relic abundance, are shown in Fig. 1. From the plot, one can identify three particularly interesting regions (see also, *e.g.*, Refs. [4, 33]): 1) the 'funnel' region, 2) the resonance region and 3) the 'tail' region, which will all be discussed in detail now.

1) For DM masses $m_{\text{DM}} < m_h/2$, the process $HH \to h^* \to b\bar{b}$ dominates, mediated by an off-shell SM Higgs boson and governed by the hHH interaction strength $\sim v\lambda_{345}$. Thus, $\Omega h^2 \propto |\lambda_{345}|^{-2}$. Since the annihilation cross section increases by approaching the resonance pole at half of the SM Higgs mass, the relic abundance decreases. The curve for the full relic abundance is symmetric with respect to zero coupling.

2) The annihilation of two DM particles into an on-shell SM Higgs boson is favoured at half the SM Higgs boson mass $m_h/2 \approx 62.5$ GeV, resulting in a large, resonantly enhanced, cross section. That leads to a relic abundance comparable to the measured value for very small portal couplings only.
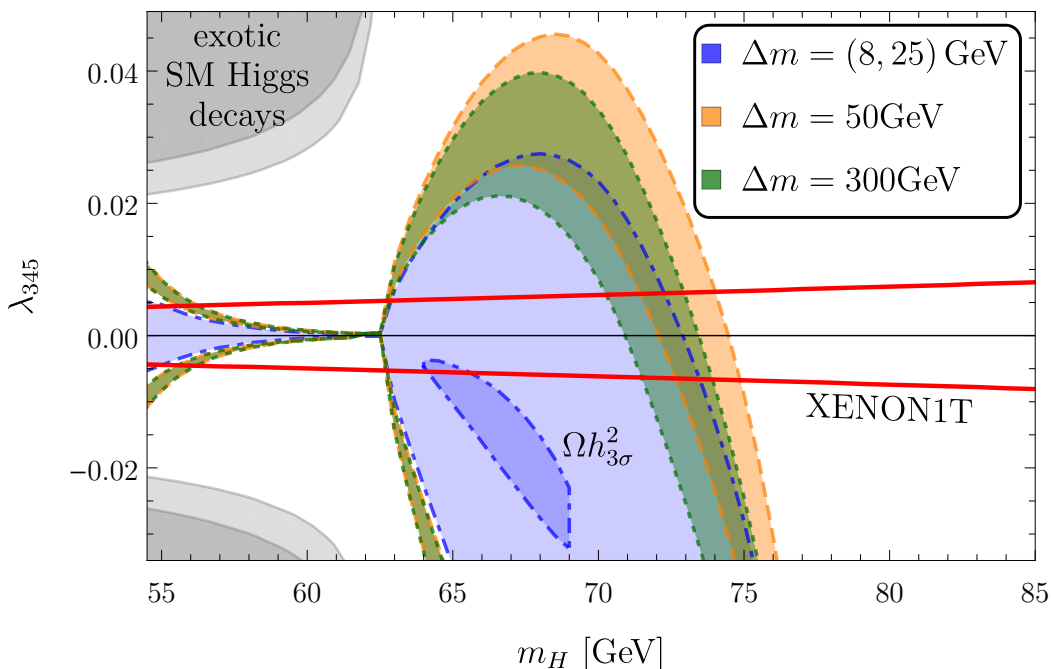

Figure 1. Contours of relic abundance within $0.6\Omega h^2_{\text{best}}$ (outer lines) and $\Omega h^2_{\text{best}} + 3\sigma$ (inner lines) for different mass splittings $\Delta m \equiv m_{A,H^\pm} - m_H$. For the smallest splitting $\Delta m = (8,25)$ GeV $= (m_A - m_H, m_{H^\pm} - m_H)$, the inner contour encloses the region with an abundance of at least $\Omega h^2_{3\sigma} \equiv \Omega h^2_{\text{best}} - 3\sigma$. Constraints from the absence of exotic SM Higgs decays for $m_H < m_h/2$ and the recent XENON1T results, indicated by the red line, reduce the viable parameter space.

3) For DM masses $m_H \gtrsim m_h/2$, contributions from annihilation processes featuring (off-shell) gauge bosons become significant (we will comment on co-annihilations via intermediate weak bosons further below). Consequently, the amplitude is not simply proportional to λ_{345} any more and interference effects occur. The closer the DM mass gets to the gauge boson mass, the stronger the contribution. In consequence, the coupling parameter λ_{345} needs to become negative to cancel the contributions of additional annihilation channels. The process $HH \to W^+ f \bar{f}'$, with an off-shell W^--boson decaying into a fermion-antifermion pair (e.g., $W^{-*} \to e^- \bar{\nu}_e$), occurs either via a four-point interaction with an SM gauge-coupling strength or via s-, t- or u-channel with an intermediate SM Higgs h or a H^-, respectively. The same holds for $HH \to Z^* Z$ with possible A-mediated channels.

Imposing constraints from searches for exotic SM Higgs decays and from the XENON1T experiment, the surviving parameter space resides in the DM mass range 55 GeV $\lesssim m_H \lesssim$ 75 GeV and in the Higgs portal coupling range $|\lambda_{345}| \lesssim 0.01$, with the latest DD limits removing significant portions of parameter space.

A comment is in order regarding the small splitting scenario, where we considered two splittings of $m_A - m_H = 8$ GeV, not to violate Eq. (1.11), and $m_{H^\pm} - m_H = 25$ GeV. The sizable second splitting suppresses co-annihilations, discussed in detail below, that otherwise would lead to significantly under-abundant DM. This allows for a new scenario for light DM at $m_H \gtrsim m_h/2$ in the IDM, where a fair DM abundance is not limited to small tuned regions.

Beyond that, an additional parameter-space region with the correct relic abundance opens in the high-mass regime $m_H \gtrsim 600$ GeV, in particular for small mass splittings $\Delta m \lesssim$ 10 GeV. The latter tendency can be understood, noting that the amplitudes for the crucial annihilation channels into longitudinal W and Z bosons scale as λ_3 and $\bar{\lambda}_{345}$, respectively. Inspecting Eqs. (1.3) and (1.5), it becomes evident that both of these couplings can become small for small Δm (given that λ_{345} is not too large). This allows for a suppressed annihilation and in turn for an appreciable DM abundance. A detailed study of this mass regime in the context of DM can be found in, e.g., Ref.[4], and we will add the connection with the emerging EWPhT towards the end of this article. We also note that the presence of the $D = 5$ operator $\mathcal{O}_{H_2 \tilde{F}}$ from Eq. (1.6) would have an impact on that region, modifying the annihilation of DM into W bosons. It would be very interesting to include this effective operator in the analysis with a proper coefficient inducing sufficient CP violation to make baryogenesis fully viable, which might also have a welcome impact on the relic abundance via destructive interference. This would, however, require significant changes in the analysis tools and is thus left for future work.

In Fig. 2, the behavior of the effective thermally averaged cross section in dependence on the mass splitting Δm is analyzed for a fixed DM mass of $m_H = 65$ GeV and two values of the portal parameter, $\lambda_{345} = -0.04$ and $\lambda_{345} = 0.02$. The upper panel shows the total cross section, which is largely enhanced due to significant co-annihilations for small mass splittings, allowing for simultaneous non-negligible presence of two $\mathbb{Z}_2$-odd states around freeze-out. This behavior is similar for both portal-coupling values, where around $\Delta m \approx 30$ GeV the steep decrease ends. For sizable splittings, $\langle \sigma_{\text{eff}} v \rangle$ approaches quickly a constant value for $\lambda_{345} = -0.04$, whereas for $\lambda_{345} = 0.02$ it first starts to increase and reaches a higher plateau for large Δm. Indeed, the contributions from co-annihilation channels become irrelevant for increased mass splitting, as can be seen in Eq. (2.3) where a large splitting results in a small fraction of the non-DM particle in the particle density at thermal equilibrium.
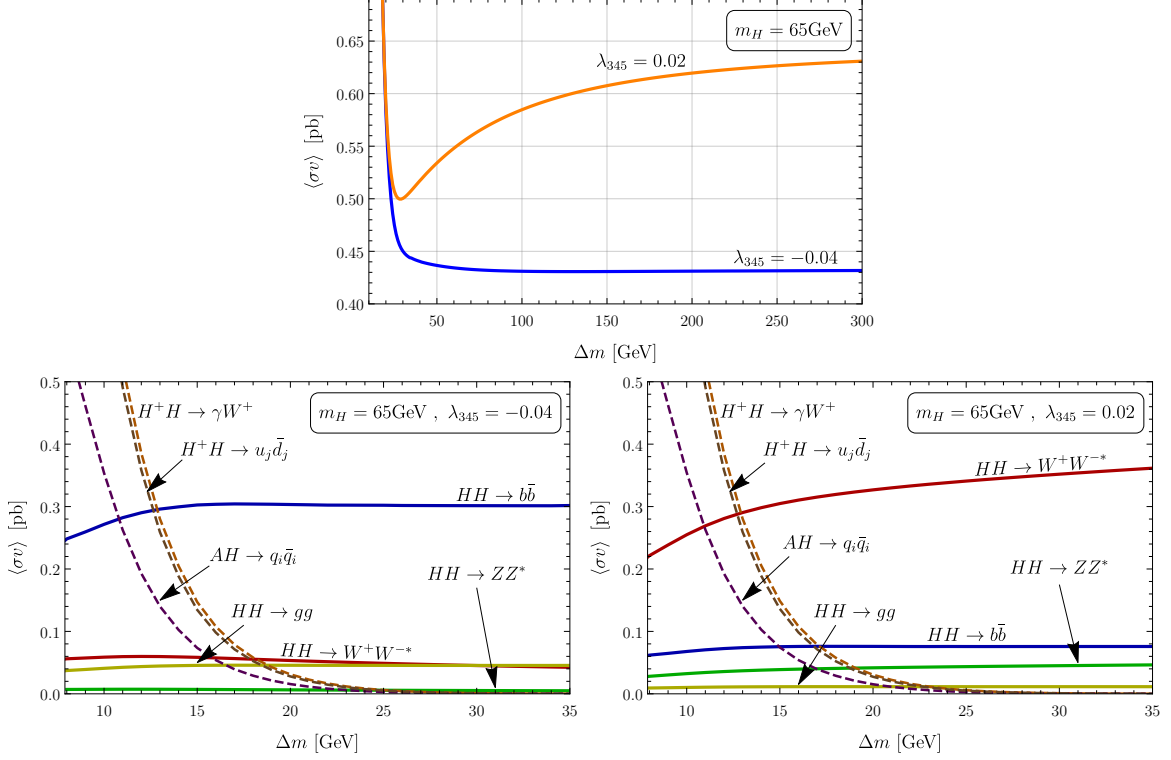
Figure 2. Dependence of the thermally averaged cross section on the mass splitting Δm for fixed DM mass $m_H = 65\,\text{GeV}$ and two Higgs portal couplings, $\lambda_{345} = -0.04, 0.02$. UPPER ROW: Total (co-)annihilation cross sections. LOWER ROW: Comparison of (co-)annihilation channels. At small mass splitting, co-annihilations (dashed) into γW^+ and quarks dominate, while the annihilation channels (solid) dominate for large Δm.

The relative differences between the various co-annihilation processes are dissected in the lower panel of Fig. 2. They are determined by the mass of the potential mediator and the coupling of the SM boson. The same is true for the DM annihilation into a $b\bar{b}$-pair via an intermediate SM-Higgs boson. On the other hand, the pair creation of SM gauge bosons $W^{\pm}$, Z can occur via a four-point interaction. One can conclude from the plots in the lower row that co-annihilation processes can become important in the considered DM mass range for small splittings. In fact, for small overall $\Delta m \lesssim 10\,\text{GeV}$, they would lead unavoidably to underabundance in the intermediate mass range of $m_H \sim 65 - 75\,\text{GeV}$. However, allowing for somewhat heavier $H^{\pm}$ while keeping m_A close to m_H can suppress the more dangerous $H^{\pm}$ co-annihilations sufficiently to allow for a low-splitting dark matter scenario in agreement with LEP constraints and achieving the full DM abundance, as envisaged before, in the context of Fig. 1.

3 Scanning the Nature of the Electroweak Phase Transitions

After having identified viable parameter-space regions for DM, the goal of this section is to investigate different kinds of EWPhT emerging in the surviving parameter space. Considering the constraints from the relic abundance and DD limits from Fig. 1, we first focus on the low DM-mass range $55\,\text{GeV} \leq m_H \leq 75\,\text{GeV}$ - the high-mass regime will be explored further below. The dependence of the type of EWPhT on the degenerate masses $m_A = m_{H^{\pm}}$ of the

$\mathbb{Z}_2$-odd non-DM particles is visualised in Fig. 3 for $\lambda_2 = 0.4$. Considering DM physics, the Higgs portal coupling λ_{345} is adapted to obtain the measured relic abundance in agreement with XENON1T limits. Regions where this is not possible and the correct abundance cannot be obtained, given DD constraints, are shaded in gray (c.f. Fig. 1). Since the type of EWPhT is rather insensitive to λ_{345} in the considered ranges of $\lambda_{345} \lesssim 0.005$ and $55\,\mathrm{GeV} < m_H < 75\,\mathrm{GeV}$, we used a fixed $\lambda_{345} = 0.005$ for the EWPhT part of the plot. The different kinds of transition are depicted by different colors, where the two-step EWPhT is strongly first-order implicitly. Finally, the critical temperature T_c and the strength of the EWPhT ξ are indicated by dotted and dashed contours, respectively.

A large range in $m_{A,H^\pm}$ with a strong first-order one-step EWPhT, *i.e.*, $\xi \geq 1$, is present (green region), while a narrow mass range allows a viable strong two-step EWPhT, not conflicting other constraints (yellow stripe). The latter had not been found before in the literature, since corresponding analyses did not consider a sizable splitting of $\Delta m \gtrsim 250\,\mathrm{GeV}$ (see, *e.g.*, Ref. [34]) and/or dense enough scan. The presented fine-grained numerical treatment enables to resolve this small range of mass splitting. Varying both λ_2 and λ_{345}, we still found that only a small window remains for the future exploration of the two-step EWPhT, regardless of the coupling parameters above. Finally, there is an upper bound for the mass splitting, beyond which the EW vacuum at zero temperature is no longer at $(v, 0) = (246, 0)$ GeV, as indicated by the light-blue region.

From Fig. 3 we choose four benchmarks (BMs), two of which lead to a strong first-order EWPhT and the other two exhibit a two-step EWPhT. The mass spectra together with a proper coupling parameter λ_{345}, inducing the correct relic abundance while eluding XENON1T DD limits, are given in Tab. 1. The small portal couplings for the BMs are due to the strong upper limits on $\sigma_{n,p}$, which can only be obeyed by tiny $|\lambda_{345}|$. In particular the BMs with two-step transitions will be promising targets for an analysis of GW signatures in the future, in the spirit of Ref. [35].

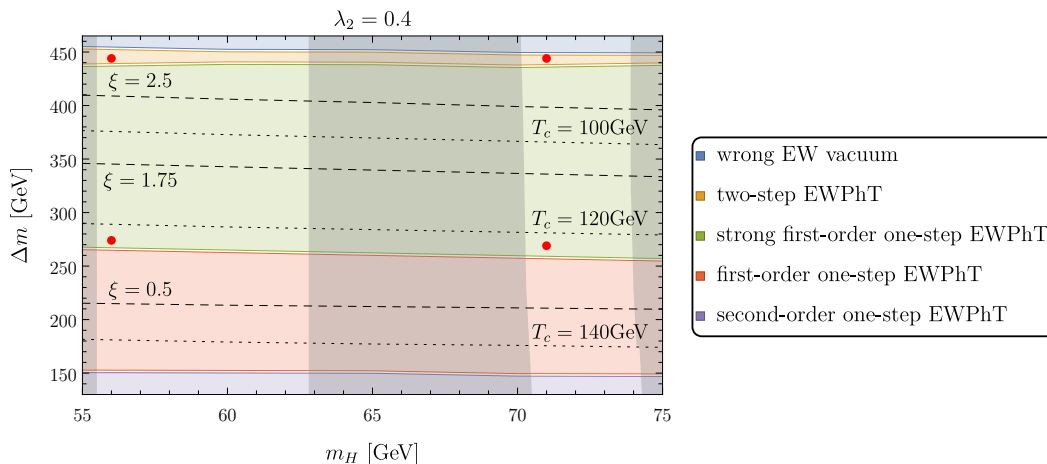The evolution of the SM Higgs field h and of the non-SM field H as the universe cools

Figure 3. Characterization of the EWPhT (colored stripes), indicating the surviving parameter space (bright regions) which provides a significant amount of the measured DM abundance, *i.e.*, $0.6\Omega h^2_{\mathrm{best}} \leq \Omega h^2 \leq \Omega h^2_{\mathrm{best}} + 3\sigma$, and obeys the latest DD limits from XENON1T, adjusting $\lambda_{345} \lesssim 0.005$. The red points denote the selected BMs (see Tab. 1), while dashed and dotted contours show the EWPhT strength ξ and the critical temperature T_c, respectively. See text for details.

BM	m_H [GeV]	$m_{A,H^\pm}$ [GeV]	λ_{345}	Ωh^2	σ_n $[10^{-13}\text{pb}]$	σ_p $[10^{-13}\text{pb}]$
1	56	330	0.0037	0.1188	379.7	372.2
2	56	500	0.0037	0.1188	379.7	372.2
3	71	340	0.0020	0.1174	69.5	68.1
4	71	515	0.0020	0.1201	69.5	68.1

Table 1. Benchmark points for the further investigation of the EWPhT dynamics. The relic abundance is within 3σ around Ωh^2_{best} and the cross sections $\sigma_{n,p}$ for scattering off a neutron or a proton, respectively, obey the latest XENON1T constraints.

down is visualized in Fig. 4 for the four BMs in Tab. 1, showing the characteristic trajectories for one-step (blue) and two-step (yellow) EWPhTs. Solid lines correspond to a smooth evolution of the fields, while dashed lines indicate a non-continuous step from the initial to the final point. In the case of a one-step EWPhT, the scalar field H does not acquire a vev different from zero, which is thus given by a straight line. Starting in the symmetric field configuration at the origin for sufficiently high temperatures, here the transition occurs at $T = T_c$. For $T < T_c$, the vacuum continues to evolve continuously towards the correct EW vacuum at $(v, 0)$. For a two-step EWPhT, $\langle H \rangle$ is non-zero within a certain temperature interval, leading to a departure from a straight line. In this scenario, the first transition happens at $T = T_1$. After a continuous evolution of the field the second transition takes place at $T = T_2 < T_1$ before the vacuum evolves continuously towards the correct one. For this, it is necessary to distinguish between two temperature-dependent strengths $\xi_1 (T_1)$ and $\xi_2 (T_2)$ in the two-step EWPhT case, see Eq. (1.31). The type of the EWPhT and the corresponding EWPhT strengths ξ_j for the BMs are summarized in Tab. 2. The strength ξ_j depends both on the mass splitting Δm and on the parameter λ_2 that is not relevant in the DM analysis as we consider tree-level processes only. Thus, it is interesting to study the impact of these two quantities on the EWPhT. In the further analysis, we use the DM mass m_H and the coupling parameter λ_{345} of BM1 and BM3 to examine the dependence of the EWPhT strength on Δm and λ_2.

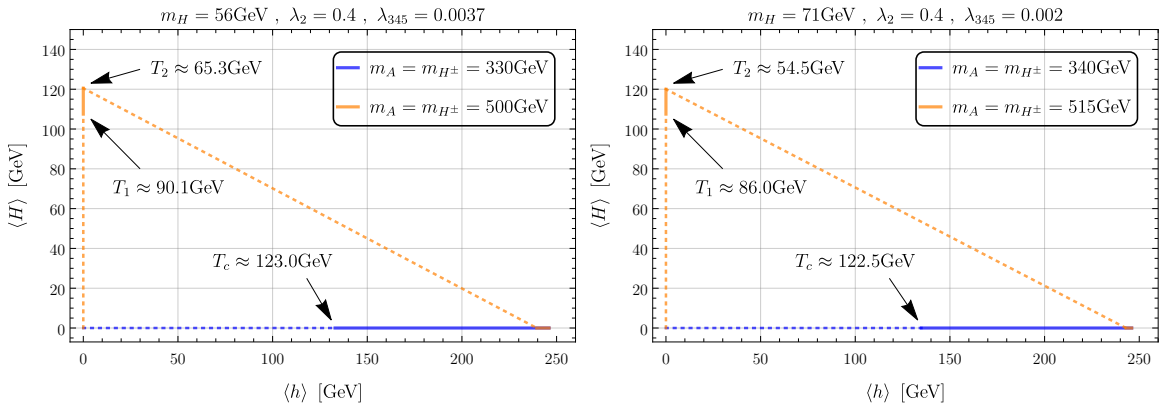In Fig. 5, the EWPhT strength ξ_j both for one-step and for two-step EWPhT as well

Figure 4. Evolution of the fields for the BMs. Solid lines correspond to a smooth evolution of the fields values, while dashed lines indicate a non-continuous transition. For the one-step EWPhT, the transition occurs around the critical temperature, denoted by T_c, while for the two-step EWPhT there are two temperatures, T_1 and T_2, for the first and second transition, respectively.
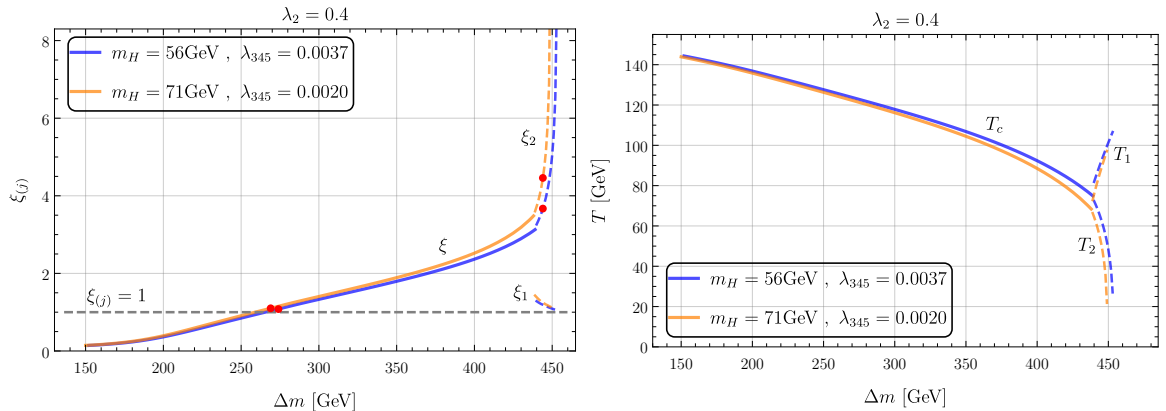
Figure 5. Evolution of the EWPhT strengths ξ_j and temperatures for different mass splittings Δm. Solid lines correspond to first-order EWPhTs whereas dashed lines to two-step EWPhTs. The EWPhT for $\Delta m \lesssim 150$ GeV is of second order and for $\Delta m \gtrsim 450$ GeV the EW vacuum does not match the proper $(v, 0) \approx (246, 0)$ GeV.

as the transition temperatures are shown. In accordance with Fig. 3, the EWPhT strength grows for increasing mass splitting. This behaviour holds both for one-step and for the second transition in the two-step EWPhT. The reason for that is the increase of the critical field value when the transition happens, together with the decrease of critical temperature, *i.e.*, the EWPhT occurs at later times. Although the range of mass splittings in which a two-step EWPhT occurs is rather small, ξ_2 increases quickly, resulting in a large ξ_2 for the considered BMs. The EWPhT strength ξ_1, corresponding to the first transition where $\langle H \rangle \neq 0$, is smaller than ξ_2 due to the different transition temperatures.

The dependence of the two-step ξ_j on the coupling λ_2 is shown in Fig. 6 for the two corresponding BMs, together with transition-temperature information. The parameter λ_2 is not completely free, as it is constrained from below by the EW vacuum condition. For sufficiently small λ_2, the global potential minimum is not located at $(v, 0)$ and is thus excluded. The exact value depends on the considered parameter set. Small values of λ_2 are favored to move from a one-step to a two-step EWPhT via large thermal corrections. We note that very large values of $\xi_2 \gtrsim 5$ are linked to rather low transition temperatures of $T_2 \lesssim 50$ GeV.

Before concluding, we go back to the high DM-mass regime, $m_H \gtrsim 600$ GeV. Here we expect it to be more difficult to simultaneously achieve a (strong) first-order EWPhT together with an appreciable DM abundance. The reason it that, as explained before in Sec. 2, in this regime for significant mass splittings, *i.e.*, sizable λ_3 and $\bar{\lambda}_{345}$, the annihilation into longitudinal W and Z bosons is large and the relic abundance is expected to be negligible. On the other hand this is the parameter space that is most promising for a strong EWPhT (*c.f.* Fig. 3). Still, this expectation is to be checked quantitatively (also because non-trivial

BM	m_H [GeV]	$m_{A,H^\pm}$ [GeV]	λ_{345}	EWPhT type	$\xi_{(1)}$	ξ_2
1	56	330	0.0037	strong first-order one-step	1.08	−
2	56	500	0.0037	two-step	1.19	3.67
3	71	340	0.0020	strong first-order one-step	1.10	−
4	71	515	0.0020	two-step	1.25	4.46

Table 2. Type and strength of the EWPhT for the four BMs, assuming $\lambda_2 = 0.4$.

cancellation could appear) and even a modest contribution of H to the DM could be interesting for prospects of DD experiments, depending on the model parameters. Like this, a potential agent of electroweak baryogenesis could still be seen in DM searches.

Thus, in Fig. 7, we present a similar characterization of the interplay of the EWPhT and DM physics as in Fig. 3, but now for heavy DM. While the color code remains the same as before, we now indicate, via dashed contours, the fraction of the full relic abundance Ωh^2_{best} that resides in H, assuming $\lambda_2 = 0.4$ and $\lambda_{345} = -0.1$, which is well below the XENON1T bound. One can inspect that achieving a large fraction of the DM abundance would only be possible in the case of a second-order transition. On the other hand, a strong first order EWPhT would still be compatible with H furnishing $\gtrsim 0.1\%$ of the DM. Finally, we note that very large mass splittings, approaching the upper boundary of the shown parameter space, correspond to low transition temperatures $T_c \lesssim 50$ GeV and should be taken with a grain of salt since DM freezeout could occur before the EWPhT. A corresponding dedicated analysis, taking this into account, would be worthwhile and could lead to interesting results. We will leave this for future work.

4   Conclusion

In this article, we investigated the prospects to realize the found DM abundance in the IDM, while taking theoretical and the latest experimental constraints into account, considering also regions of parameter space not explored in detail before. We found that the tight limits from XENON1T constrain the DM mass to the range 55 GeV $\lesssim m_H \lesssim 75$ GeV together with a small Higgs portal coupling $|\lambda_{345}| \lesssim 0.01$ or to a high mass regime of $m_H \gtrsim 500$ GeV. In the low mass range, we found a new viable spectrum for a realistic DM abundance, considering a small, but non-universal, splitting of $\Delta m = (8, 25)$ GeV. To arrive at this conclusion, the behavior of the cross sections of several (co-)annihilation channels was analyzed in detail.

Afterwards, the surviving parameter space was studied in light of the EWPhT and we chose four BMs for an in-depth analysis of the evolution of the vacuum while the temperature decreases. The dependence of the EWPhT strengths $\xi_{(j)}$, both on the mass splitting and the coupling parameter λ_2, along with the behaviour of the transition temperature for different mass splittings were examined in detail. For the light-DM scenario, we discovered a broad mass range for the non-DM $\mathbb{Z}_2$-odd particles that leads to a strong first-order EWPhT either
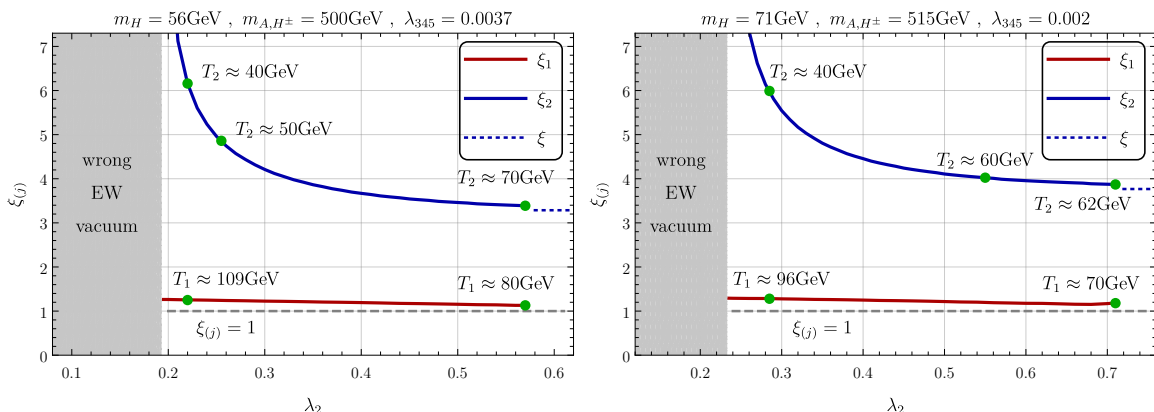

Figure 6. Dependence of ξ_j on the coupling parameter λ_2 for two BMs which represent two-step EWPhTs. The red lines correspond to ξ_1, *i.e.*, the first transition, and the blue lines to ξ_2.
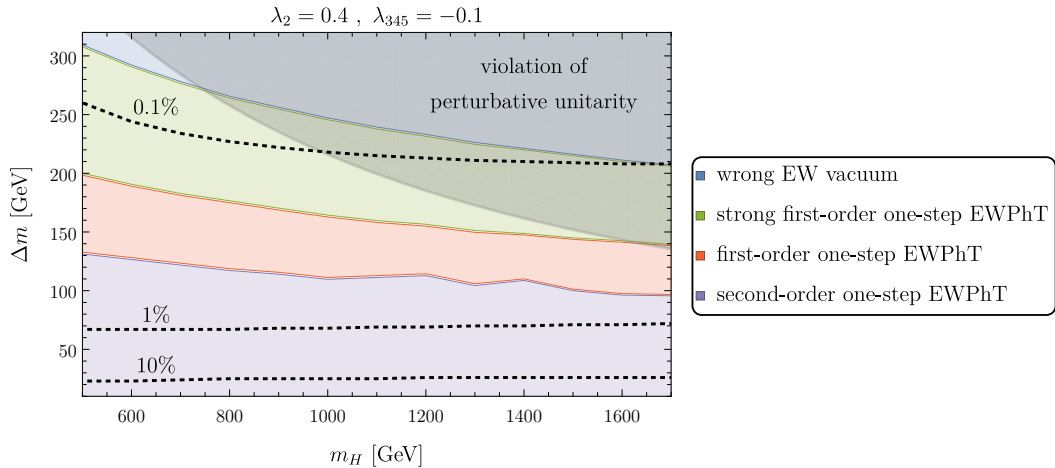
Figure 7. Characterization of the EWPhT (colored stripes) for the high-mass regime. The dashed contours indicate the fraction of the full relic abundance Ωh^2_{best} that resides in H. See text for details.

via one step or via two steps during the evolution of the universe. For the heavy-DM regime the phase transition seems generically to be second-order, unless H only represents a sub-population of DM. These quantitative findings, and in particular the characteristic two-step EWPhT, can be probed by investigating GW signatures. A detailed analysis in this direction is left for future work.

Acknowledgments

References

[1] M. Tanabashi et al. (Particle Data Group), *Big-bang cosmology, Phys. Rev. D 98, 030001* (2019) .

[2] L.L. Honorez, E. Nezri, J.F. Oliver and M.H.G. Tytgat, *The inert doublet model: An archetype for dark matter, Journal of Cosmology and Astroparticle Physics* **2007** (2007) 028 [hep-ph/0612275v2].

[3] R. Barbieri, L.J. Hall and V.S. Rychkov, *Improved naturalness with a heavy higgs: An alternative road to lhc physics, Physical Review D* **74** (2006) [hep-ph/0603188v2].

[4] Alexander Belyaev et al., *Anatomy of the inert two higgs doublet model in the light of the lhc and non-lhc dark matter searches, Physical Review D* **97** (2018) [1612.00511v1].

[5] A. Sakharov, *Violation of CP Invariance, C asymmetry, and baryon asymmetry of the universe, Sov. Phys. Usp.* **34** (1991) 392.

[6] B. Grzadkowski, O. Ogreid, P. Osland, A. Pukhov and M. Purmohammadi, *Exploring the CP-Violating Inert-Doublet Model, JHEP* **06** (2011) 003 [1012.4680].

[7] M. Krawczyk, N. Darvishi and D. Sokolowska, *The Inert Doublet Model and its extensions, Acta Phys. Polon. B* **47** (2016) 183 [1512.06437].

[8] A. Cordero-Cid, J. Hernández-Sánchez, V. Keus, S. Moretti, D. Rojas-Ciofalo and D. Sokołowska, *Collider signatures of dark CP-violation*, *Phys. Rev. D* **101** (2020) 095023 [2002.04616].

[9] M. Dine, P. Huet, J. Singleton, Robert L. and L. Susskind, *Creating the baryon asymmetry at the electroweak phase transition*, *Phys. Lett. B* **257** (1991) 351.

[10] M. Dine, P. Huet and J. Singleton, Robert L., *Baryogenesis at the electroweak scale*, *Nucl. Phys. B* **375** (1992) 625.

[11] C. Balazs, G. White and J. Yue, *Effective field theory, electric dipole moments and electroweak baryogenesis*, *JHEP* **03** (2017) 030 [1612.01270].

[12] F. Ferreira, B. Fuks, V. Sanz and D. Sengupta, *Probing CP-violating Higgs and gauge-boson couplings in the Standard Model effective field theory*, *Eur. Phys. J. C* **77** (2017) 675 [1612.01808].

[13] T. Alanne and F. Goertz, *Extended Dark Matter EFT*, *Eur. Phys. J. C* **80** (2020) 446 [1712.07626].

[14] Agnieszka Ilnicka et al., *Inert Doublet Model in light of LHC Run I and astrophysical data*, *Physical Review D* **93** (2016) [1508.01671v2].

[15] E. Lundström, M. Gustafsson and J. Edsjö, *Inert Doublet Model and LEP II Limits*, *Physical Review D* **79** (2009) [0810.3924v2].

[16] A. Pierce and J. Thaler, *Natural dark matter from an unnatural higgs boson and new colored particles at the TeV scale*, *Journal of High Energy Physics* **2007** (2007) 026 [hep-ph/0703056v2].

[17] M.E. Peskin and T. Takeuchi, *New constraint on a strongly interacting higgs sector*, *Physical Review Letters* **65** (1990) 964.

[18] M. Baak, , J. Cúth, J. Haller, A. Hoecker, R. Kogler et al., *The global electroweak fit at nnlo and prospects for the lhc and ilc*, *The European Physical Journal C* **74** (2014) [1407.3792v1].

[19] M. Aaboud, G. Aad, B. Abbott, D. Abbott, O. Abdinov, A.A. Abud et al., *Combination of searches for invisible higgs boson decays with the ATLAS experiment*, *Physical Review Letters* **122** (2019) .

[20] CMS Collaboration, *Search for invisible decays of a higgs boson produced through vector boson fusion in proton-proton collisions at $\sqrt{s} = 13$ tev*, *Physics Letters B* **793** (2019) 520 [1809.05937v3].

[21] M. Tanabashi et al. (Particle Data Group), *Status of higgs boson physics*, Phys. Rev. D 98, 030001 (2018) .

[22] J.M. Cline, K. Kainulainen and M. Trott, *Electroweak baryogenesis in two higgs doublet models and b meson anomalies*, *Journal of High Energy Physics* **2011** (2011) [1107.3559v3].

[23] L. Dolan and R. Jackiw, *Symmetry behavior at finite temperature*, *Physical Review D* **9** (1974) 3320.

[24] G.W. Anderson and L.J. Hall, *Electroweak phase transition and baryogenesis*, *Physical Review D* **45** (1992) 2685.

[25] Yun Jiang et al., *A new insight into the phase transition in the early universe with two higgs doublets*, *Journal of High Energy Physics* **2018** (2018) [1712.08430v3].

[26] D.J. Gross, R.D. Pisarski and L.G. Yaffe, *QCD and instantons at finite temperature*, *Reviews of Modern Physics* **53** (1981) 43.

[27] R.R. Parwani, *Resummation in a hot scalar field theory*, *Physical Review D* **45** (1992) 4695.

[28] J. Edsjö and P. Gondolo, *Neutralino relic density including coannihilations*, *Physical Review D* **56** (1997) 1879.

[29] Paolo Gondolo et al., *Cosmic abundances of stable particles: Improved analysis*, *Nuclear Physics B360* (1991) 145.

[30] D. Barducci et al., *MicrOMEGAs: The user's manual, version 5*.

[31] A. Pukhov, A.Belyaev, N. Christensen, *CalcHEP Calculator for High Energy Physics*, 2012.

[32] P.A. Zyla et al. (Particle Data Group), *Astrophysical constants and parameters*, *Prog. Theor. Exp. Phys.* (2020) .

[33] N. Blinov, S. Profumo and T. Stefaniak, *The Electroweak Phase Transition in the Inert Doublet Model*, *JCAP* **07** (2015) 028 [1504.05949].

[34] G. Gil, P. Chankowski and M. Krawczyk, *Inert Dark Matter and Strong Electroweak Phase Transition*, *Phys. Lett. B* **717** (2012) 396 [1207.0084].

[35] A.P. Morais and R. Pasechnik, *Probing multi-step electroweak phase transition with multi-peaked primordial gravitational waves spectra*, *JCAP* **04** (2020) 036 [1910.00717].